Indian Journal of
METEOROLOGY & GEOPHYSICS

JANUARY 1973
Vol. 24 No. 1

551.553.21: 003.54 (322.54)

Numerical simulation of the Indian summer monsoon

R. V. GODBOLE

Indian Institute of Tropical Meteorology, Poona

(*Received 4 January 1972*)

ABSTRACT. A simplified model of zonally symmetric motion in the two-dimension has been formulated to simulate the monsoon circulation. The atmosphere from the surface upto the top has been divided into nine levels for which temperature, water vapour and velocity components are predicted. The final solution is obtained as the asymptotic steady state of an initial value problem solved by a marching process.

To start with, the atmosphere was assumed to be at rest. As time progressed, winds slowly developed. After 80 days, the simulated circulation was fully developed, as normally observed, with westerlies in the lower levels and easterlies aloft. The easterly jet had a core speed of 35 m/sec. The meridional circulation showed southerlies near the surface and northerlies at higher levels.

The circulation was found to become weak when the presence of the Himalayas was disregarded. The upper-level easterlies reached a maximum speed of hardly 8 m/sec. Neglect of moisture in the model did not affect the monsoon circulation, although its presence was essential for the occurrence of rainfall. On the whole, the results bring out the importance of thermal and dynamical influence of the Himalayas upon the generation and the development of the monsoon circulation.

1. Introduction

The feasiblity of numerically simulating the general circulation was first demonstrated by Phillips (1956). The properties of the general circulation and the processes which contribute towards its maintenance have been investigated by numerical methods by Smagorinsky *et al.* (1965) and by Manabe *et al.* (1965, 1970). The studies by these investigators, as well as by others (Mintz and Arakawa 1963; Mintz 1965; Leith 1965; Holoway *et al.* 1971) took into account the features of the general circulation that are observed on a global scale. The Indian summer monsoon, with its characteristic southwesterly current in the lower troposphere and a marked easterly flow above 500 mb, forms an important part of the general circulation in the tropics. It is well suited for study by numerical methods, even though various aspects of it have been studied by synoptic means. In this paper, we attempt a modelling experiment on the Indian summer monsoon.

2. Methodology of simulation

In this model, zonally symmetric motion was considered in a two dimensional vertical plane along 80°E. No disturbance was superimposed upon the zonal current. The region extending from the equator upto the north pole has been considered. In the horizontal, 18 grid-points at 5-degree latitude intervals were used (Fig. 1 a). In the verical, the sigma (σ) system of coordinates was used to simplify the inclusion of topography. The free atmosphere has been divided into eight levels. The top of the friction layer coincided with level '$8\frac{1}{2}$' and the ground was represented by level '9' (Fig. 1 b). For further details a reference may be made to Godbole *et al.* (1970). The latitudinal dependence of sigma-levels is shown in Fig. 2. For convenience, the northern boundary of the Indian Ocean was fixed at 15°N. The region corresponding to the top of the Himalayas coincided with latitude 32·5°N.

The experiment was performed for the following sets of conditions : (1) with moisture and with the Himalayas (wet model with the Himalayas), (2) without moisture and with the Himalayas (dry model with the Himalayas), (3) without moisture and without the Himalayas (dry model without the Himalayas), and (4) with moisture and without the Himalayas (wet model without the Himalayas). Experiment (3) was subdivided with respect to

two preassigned sea surface temperatures, namely, 300° and 290°K. Experiment (4) was also subdivided according to two different surface mixing ratio values, namely, 80 and 40 per cent of saturation mixing ratio at the surface, and also by the assumption that condensation occurred at 80 per cent relative humidity.

Using a finite difference scheme, which was designed to conserve energy, the solution was obtained by a marching process. Initially the atmosphere was assumed to be dry ($r=0$) and at rest ($u=v=w=0$). The temperature distribution in the vertical was obtained from the U.S. standard atmosphere (US Air Force 1962). The time interval of integration was taken as 10 minutes; consequently, the integration time of one day corresponded to 144 time steps. The marching process was continued until an equilibrium was reached, when the change of u, v, and T with respect to time was sufficiently small. In practice,equilibrium was considered to have been reached when the difference between the daily mean temperatures simulated of two consecutive days was less than 0·1°C. It was observed that equilibrium was attained in about 80 days.

3. Symbols

The symbols used in this paper are as follows :

p_* pressure at the earth's surface
p pressure at any level
ϕ latitude
σ p/p_*
σ° $d\sigma/dt$
u zonal wind velocity
v meridional wind velocity
T temperature
r mixing ratio of water vapour
Φ geopotential height of sigma-surface
ω dp/dt
q° rate of non-adiabatic heating (radiation and condensation)
F_λ frictional effect in the zonal direction due to horizontal and vertical diffusion of momentum
F_ϕ frictional effect in the meridional direction due to horizontal and vertical diffusion of momentum
F_T effect of horizontal and vertical diffusion of heat
F_r effect of horizontal and vertical diffusion of water vapour
C amount of condensation
f coriolis parameter
$\tau^{\lambda\lambda}$ westward diffusive flux of E-ward momentum
$\tau^{\lambda\phi}$ southward diffusive flux of E-ward momentum
$\tau^{\phi\phi}$ southward diffusive flux of N-ward momentum
γ^ϕ southward diffusive flux of heat
μ^ϕ southward diffusive flux of water vapour
$\tau^{\lambda z}$ downward diffusive flux of E-ward momentum
$\tau^{\phi z}$ downward diffusive flux of N-ward momentum
γ^z downward diffusive flux of heat
μ^z downward diffusive flux of water vapour
g accelaration due to gravity
K_H horizontal eddy diffusion coefficient
K_V vertical eddy diffusion coefficient
d grid distance in km
l mixing length
k_0 Karman constant
z_0 roughness parameter
U wind speed in the surface boundary layer
ξ wind direction
h thickness of the turbulence layer
z_* ground surface

4. Prognostic Equations

The parameters to be predicted are the velocity components (u, v), the temperature (T), and the water vapur mixing ratio (r). The equations for two-dimentional zonally symmetric motion in spherical coordinates (ϕ, λ) and the vertical coordinate (σ) may be written as (Kurihara *et al.* 1967)—

$$\frac{\partial p_* u}{\partial t} = -\frac{\partial p_* uv\cos\phi}{a\cos\phi\,\partial\phi} - \frac{\partial p_* u\sigma^\circ}{\partial\sigma} + \left(f + \frac{\tan\phi}{a}u\right)v + p_* F_\lambda \qquad (4\cdot1)$$

$$\frac{\partial p_* v}{\partial t} = -\frac{\partial\, p_* v^2\cos\phi}{a\cos\phi\,\partial\phi} - \frac{\partial p_* v\sigma^\circ}{\partial\,\sigma} - \left(f + \frac{\tan\phi}{a}u\right)v + \sigma\frac{\partial\,\Phi}{\partial\,\sigma}\frac{\partial p_*}{a\partial\phi} - p_*\frac{\partial\Phi}{a\partial\phi} + p_*\,F_\phi \qquad (4\cdot2)$$

$$\frac{\partial p_* T}{\partial t} = -\frac{\partial p_*\,Tv\cos\phi}{a\cos\phi\,\partial\phi} - \frac{\partial p_* T\sigma^\circ}{\partial\sigma} - \frac{\omega}{c_p}p_* q^\circ + p_* F_T \qquad (4\cdot3)$$

$$\frac{\partial\, p_* r}{\partial t} = -\frac{\partial\, p_*\, rv\cos\phi}{a\cos\phi\,\partial\phi} - \frac{\partial\,\, p_*\, r\sigma^\circ}{\partial\,\sigma} - p_*\,C + p_*\,F_r \qquad (4\cdot4)$$

To the above set, we add the continuity equation

$$\frac{\partial p_*}{\partial t} = -\frac{\partial p_* v\cos\phi}{a\cos\phi\,\partial\phi} - \frac{\partial p_*\sigma^\circ}{\partial\sigma} \qquad (4\cdot5)$$

and equation for hydrostatic balance

$$\frac{\partial\Phi}{\partial\sigma} = -\frac{RT}{\sigma} \qquad (4\cdot6)$$

The vertical velocity ω is

$$\omega = p_*\sigma^\circ + \sigma\left(\frac{\partial p_*}{\partial t} + v\frac{\partial p_*}{a\partial\phi}\right) \qquad (4\cdot7)$$

5. Subgrid-scale mixing

In the case of zonally symmetric motion the frictional forces in the zonal (F_λ) and meridional (F_ϕ) direction and the forces governing diffusion of heat (F_T) and water vapour (F_r) may be expressed as

$$p_* F_\lambda = \frac{\partial}{a\cos\phi\,\partial\phi}\left(\tau^{\lambda\phi}\cos^2\phi\,\frac{\partial\Phi}{\partial\sigma}\right) + \frac{\partial}{\partial\sigma}\left(\tau^{\lambda\phi}\frac{\partial\Phi}{a\partial\phi}\right) - g\frac{\partial\tau^{\lambda z}}{\partial\sigma} \qquad (5\cdot1)$$

$$p_* F_\phi = -\frac{\partial}{a\cos\phi\,\partial\phi}\left(\tau^{\phi\phi}\cos\phi\,\frac{\partial\Phi}{\partial\sigma}\right) + \frac{\partial}{\partial\sigma}\left(\tau^{\phi\phi}\frac{\partial\Phi}{a\partial\phi}\right) - \frac{\tan\phi}{a}\tau^{\lambda\lambda}\frac{\partial\Phi}{\partial\sigma} - g\frac{\partial\tau^{\phi z}}{\partial\sigma} \qquad (5\cdot2)$$

$$p_* F_T = -\frac{\partial}{a\cos\phi\,\partial\phi}\left(\gamma^\phi\frac{\partial\Phi}{\partial\sigma}\right) + \frac{\partial}{\partial\sigma}\left(\gamma^\phi\frac{\partial\Phi}{a\partial\phi}\right) - g\frac{\partial\gamma^z}{\partial\sigma} \qquad (5\cdot3)$$

$$p_* F_r = -\frac{\partial}{a\cos\phi\,\partial\phi}\left(\mu^\phi\frac{\partial\Phi}{\partial\sigma}\right) + \frac{\partial}{\partial\sigma}\left(\mu^\phi\frac{\partial\Phi}{a\partial\phi}\right) - g\frac{\partial\mu^z}{\partial\sigma} \qquad (5\cdot4)$$

where,

$$\tau^{\lambda\lambda} = -p_* K_H\left(\frac{\sigma}{RT}\right)\frac{\tan\phi}{a}v \qquad (5\cdot5)$$

$$\tau^{\lambda\phi} = -p_* K_H\left(\frac{\sigma}{RT}\right)^2\left\{\frac{\partial\Phi}{\partial\sigma}\frac{\partial}{a\partial\phi}\left(\frac{u}{\cos\phi}\right) - \frac{\partial\Phi}{a\partial\phi}\frac{\partial}{\partial\sigma}\left(\frac{u}{\cos\phi}\right)\right\}\cos\phi \qquad (5\cdot6)$$

$$\tau^{\phi\phi} = -p_* K_H\left(\frac{\sigma}{RT}\right)^2\left\{\frac{\partial\Phi}{\partial\sigma}\frac{\partial v}{a\partial\phi} - \frac{\partial\Phi}{a\partial\phi}\cdot\frac{\partial v}{\partial\sigma}\right\} \qquad (5\cdot7)$$

$$\gamma^\phi = -p_* K_H\left(\frac{\sigma}{RT}\right)^2\left\{\frac{\partial\Phi}{\partial\sigma}\frac{\partial T}{a\partial\phi} - \frac{\partial\Phi}{a\partial\phi}\frac{\partial T}{\partial\sigma}\right\} \qquad (5\cdot8)$$

$$\mu^\phi = -p_* K_H\left(\frac{\sigma}{RT}\right)^2\left\{\frac{\partial\Phi}{\partial\sigma}\frac{\partial r}{a\partial\phi} - \frac{\partial\Phi}{a\partial\phi}\frac{\partial r}{\partial\sigma}\right\} \qquad (5\cdot9)$$

$$\tau^{\lambda z} = -gp_* K_V\left(\frac{\sigma}{RT}\right)^2\frac{\partial u}{\partial\sigma} \qquad (5\cdot10)$$

$$\tau^{\phi z} = -gp_* K_V\left(\frac{\sigma}{RT}\right)^2\frac{\partial v}{\partial\sigma} \qquad (5\cdot11)$$

$$\gamma^z = -gp_* K_V\left(\frac{\sigma}{RT}\right)^2\frac{\partial T}{\partial\sigma} \qquad (5\cdot12)$$

$$\mu^z = -gp_* K_V\left(\frac{\sigma}{RT}\right)^2\frac{\partial r}{\partial\sigma} \qquad (5\cdot13)$$

The lateral and vertical eddy diffusion coefficients K_H and K_V were determined from the expressions given by (Leith 1965)

$$K_H = 6\times10^4\left(\frac{d}{300}\right)^{4/3}\ \mathrm{m^2/sec} \qquad (5.14)$$

where d is the grid distance in km.

$$K_V = l^2\frac{\partial U}{\partial z} \qquad (5\cdot15)$$

where, $U = (u^2+v^2)^{\frac{1}{2}}$

and l is the mixing length. The vertical variation of l as used by Smagorinsky (1965) was adopted, namely,

$$\left.\begin{aligned} l &= k_0(z+z_0) && z\leqslant h\\ l &= k_0(h+z_0)\frac{H-z}{H-h} && h\leqslant z\leqslant H\\ l &= 0 && H\leqslant z\end{aligned}\right\} \qquad (5\cdot16)$$

where H was assumed to be 3000 m. k_0 is Von Karman's constant (0·4) and z_0 is the roughness parameter. In the computations, the values of z_0 were considered to be 0·1, 1·0 and 10 cm for sea, land and mountain respectively.

Within the turbulence layer, we assume that the horizontal eddy stresses such as $\tau^{\lambda\lambda}$, $\tau^{\lambda\phi}$, $\tau^{\phi\phi}$, γ^{ϕ} and μ^{ϕ} are all zero and the vertical fluxes of momentum, heat, and water vapour are constant, *i.e.*,

$$\left.\begin{aligned} \frac{p_*}{\rho}\frac{\partial \tau^z}{\partial z} &= 0 \\ \frac{p_*}{\rho}\frac{\partial \gamma^z}{\partial z} &= 0 \\ \frac{p_*}{\rho}\frac{\partial \mu^z}{\partial z} &= 0 \end{aligned}\right\} \qquad (5.17)$$

where,

$$\tau^{\lambda z} = \tau^z \cos\xi, \quad \tau^{\phi z} = \tau^z \sin\xi \quad \text{and}$$

$$\xi = \tan^{-1}(v/u)$$

ξ, which denotes the wind direction, is assumed to be constant within the turbulence layer. The velocity components (u,v), temperature (T), and mixing ratio (r) at the top of the turbulence layer were computed by assuming the continuity of vertical derivatives of U, T and r at the top of the turbulence layer.

6. Radiation

Radiation was considered to be the primary force for the monsoon circulation. Its contribution (q°) appears in the fourth term on the right hand side of equation (4·3).

The heating due to both to short and long wave radiation was computed from the climatological distribution of water vapour, carbon dioxide, ozone, and cloud amount for the month of July. In other words, in estimating the radiational effect, we do not use the distribution of water vapour as predicted in equation (4·4). Again, for computing the absorption of direct as well as reflected solar radiation, it was assumed that the zenith angle of the sun remained constant with time at its mean July value. In spite of these assumptions, the radiative heating remains time dependent because of its being a function of temperature (T) which is predicted in equation (4·3). The radiation computations were repeated at intervals of six hours. The treatment for computing the absorption of solar and long wave radiation in an earlier study by Godbole *et al.* (1970) was adopted in the present study.

In the month of July, the direct solar radiation is maximum near the latitude of 35°N because the product of the duration of sunshine and the cosine of the zenith angle of the sun is maximum there. Due to the fact that the observationally determined water vapour is maximum near the latitude of 20°N in the lower troposphere, a relative radiational warming is brought about over this latitude as compared to the surrounding. Inequality in the radiational heating, therefore, exists and in order to compensate for the heat contrast, the motion will start gradually ultimately leading to the monsoon circulation.

7. Convection and Condensation

The effect of convection is incorporated in the model indirectly by adopting a simplified process (Manabe *et al.* 1965) of dry and wet convective adjustments of temperature and water vapour, as a substitute for the actual convective process. The vertical distribution of temperature in any layer of a column was adjusted to the dry (wet) adiabatic lapse rate whenever the distribution of temperature exceeded the dry (wet) adiabatic lapse rate for humidity less (more) than 100 per cent. In making the adjustment it was assumed that the kinetic energy created by convection was converted into heat instantaneously, so that the potential energy remained invariant. In wet convective adjustment, it was assumed that all the water vapour which was condensed precipitated instantaneously. The temperature was adjusted corresponding to the amount of latent heat which was released in the process of condensation.

Condensation, which occurred due to non-convective processes, was also taken into account. In any layer where the relative humidity exceeded 100 per cent with its temperature lapse rate less than the wet adiabatic lapse rate, the vertical distribution of relative humidity was adjusted to 100 per cent. As in the case of wet convective adjustment, the excess of water vapour which was condensed was assumed to precipitate instantaneously, and the temperature was adjusted corresponding to the amount of latent heat released in the process of condensation. The details are available in a paper by Murakami *et al.* (1968).

8. Boundary Conditions

The vertical boundary conditions are such that at the top and the bottom of the atmosphere, the vertical σ-velocity is zero, *i.e.*,

$$\sigma^\circ = 0, \text{ at } \sigma = 0, 1 \qquad (8\cdot1)$$

The lateral boundary conditions are introduced such that at the equator and at the pole, no transport of momentum of heat and moisture was allowed to take place, *i.e.*,

$$v=0 \text{ at the equator and the pole.} \qquad (8\cdot2)$$

In order to exclude the possibility of generation of gravity waves at the lateral boundaries, the following condition was used.

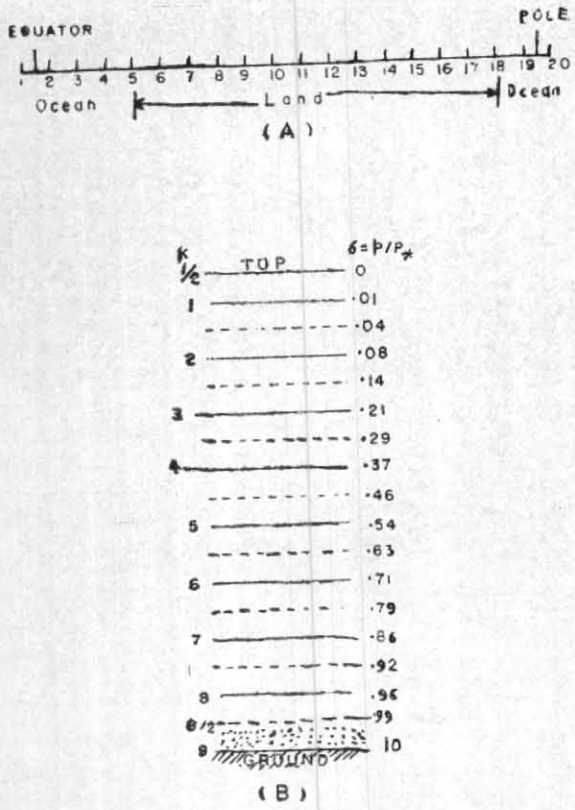

Fig. 1

(A) Horizontal grid in the N-S direction. The grid interval is 5° Lat.

(B) Various sigma-levels in the vertical

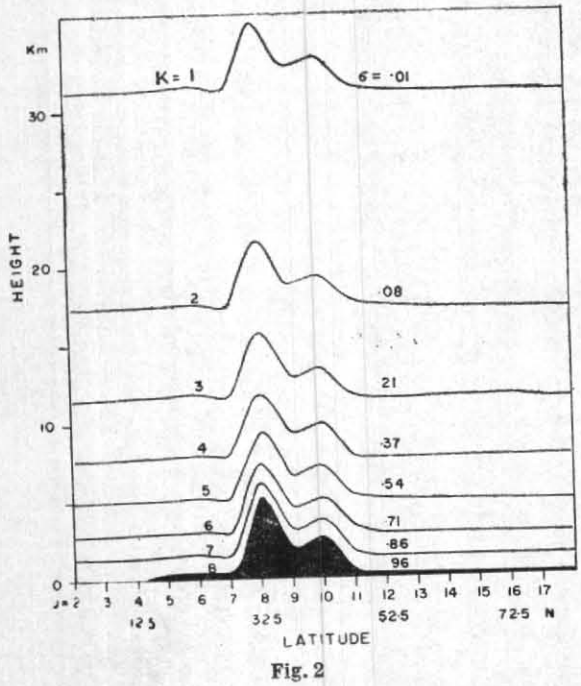

Fig. 2

Latitudinal variation of the height of the sigma-level

$u=0$, at the equator and the pole (8·3)

At the top of the atmosphere, the downward long wave radiation assumed to be zero. Solar constant was considered to be 2 ly min^{-1}.

At the earth's surface, the temperature was determined such that it satisfied the requirement of heat balance at the earth's surface. The balance equation may be written as

$$S_* + (\mathrm{DLR})_* = sT_*^4 - c_p\left(\gamma_*^z + \frac{L}{c_p}\mu_*^z \right) \quad (8\cdot4)$$

In the above, S_* and $(\mathrm{DLR})_*$ are the net downward solar radiation and the downward long wave radiation respectively at the earth's surface. s is the Stephen-Boltzman constant. $c_p\gamma_*^z$ and $L\mu_*^z$ represent the downward sensible and latent heat exchange respectively at the earth-atmosphere interface. γ_*^z and μ_*^z may be expressed in the final form as

$$\gamma_*^z = -\rho_* k_0^2 m^2 U_8 (T_* - T_8) \quad (8\cdot5)$$

and

$$\mu_*^z = -\rho_* k_0^2 m^2 U_8 (\gamma_* - \gamma_8) \quad (8.6)$$

where, $m = \left[\ln \frac{h+z_0}{z_0} + \frac{\triangle z}{h+z_0} \right]^{-1}$

In the above, the subscript * refers to the quantities at the earth's surface and the subscript 8 refers to the quantities at level 8 (*see* Fig. 1b).

9. Basic Data

9.1. *Water vapour* — The mixing ratio of water vapour was determined by using *Monthly Climate Data for the World* for July 1964-65 published by ESSA of United States. Analysis of mixing ratio at standard isobaric levels was made for the region from 0 to 90°N and from 70 to 100°E and the values were read at each grid point along 80°E. These were further plotted individually as height-temperature profiles. Mixing ratio above 500 mb was extrapolated until a line of constant frost point of 190° K was reached. Thereafter mixing ratio was assumed to follow a constant frost point of 190°K irrespective of latitude upto a height of 30 km, as considered by Manabe *et al.* (1961). Above 30 km, a constant mixing ratio line was followed.

At the earth's surface, the mixing ratio of water vapour was determined by using the relation

$$r_* = \beta r_s(T_*) \quad (9\cdot1)$$

where r_* is the mixing ratio at the earth's surface. β is a constant arbitrarily fixed and $r_s(T_*)$ is the saturation mixing ratio at the earth's surface temperature T_*. β is considered to be unity

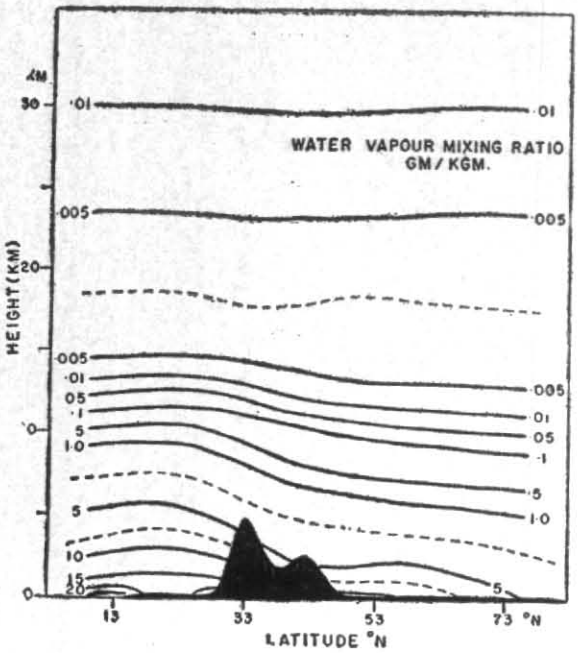

Fig. 3. Water vapour

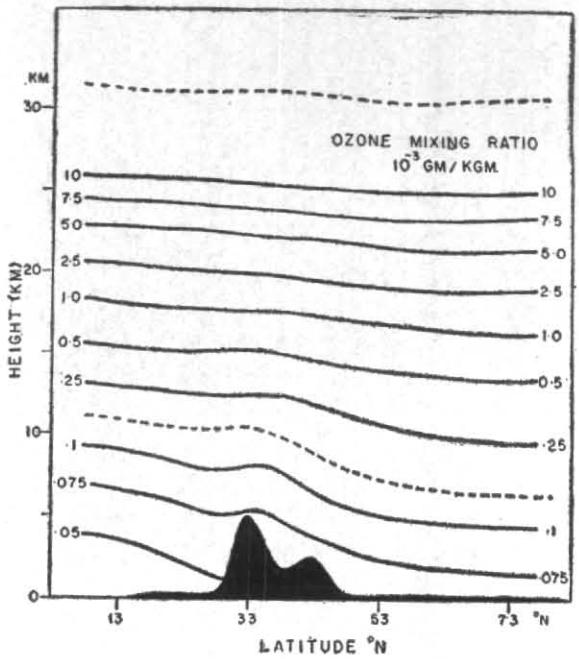

Fig. 4. Ozone

Distribution of water vapour and ozone as a function of height and latitude

for the sea surface. It was assumed to be 0·8 for the land and 0·6 for the mountain. The distribution of water vapour, thus determined, is presented in Fig. 3.

9.2. *Carbon dioxide* — The mixing ratio has been assumed to be constant at 0·456 (gm/kgm) for all the levels and for all the latitudes.

9.3. *Ozone* — The mixing ratio was determined on the basis of the *Ozone Data of the World* published by the Meteorological Service of Canada and supplemented by the cross-sections earlier published by Ramanathan and Kulkarni (1960) and Murgatroyd (1964). In Fig. 4 is shown the ozone distribution with respect to height and latitude.

9.4. *Albedo* — The values of surface albedo as given by the *Smithsonian Tables* (Table No. 154) for different surface conditions have been adopted.

9.5. *Cloud* — The cloud amount was determined by using Daily Weather Map with Synoptic Data Tabulation of Japan Meteorological Agency and the Daily Series, Northern Hemispheric Data Tabulations of the U.S. Weather Bureau. Mean cloud amount for July 1964-65 was plotted for stations within the region from 70°E to 100°E and from equator to north pole. After analysing the values were picked up at the grid points along 80°E.

9·6. *Absorptivity and emissivity* — The values of mean slab absorptivity and emissivity for water vapour, carbon dioxide and ozone and also the values of absorption of solar radiation by these gases, as given by Manabe and Moller (1961) have been used.

10. Results and Discussions

As the monsoon activity is limited to the south of the Himalayas, results are presented for the region from equator to 40°N.

10.1. *Wet model with the Himalayas* — Evaporation at the earth's surface (corresponding to $\beta = 0{\cdot}8$ in Eq. 9·1) and condensation in the free atmosphere have been considered. Fig. 5 shows the distribution of simulated zonal wind with respect to height and latitude. The essential features which are indicated are the existence of (1) a tropical easterly jet (TEJ) at 12 km with core speed of 36 m sec^{-1} at 20°N and (2) low-level westerly of more than 10 m sec^{-1} extending from south of the Himalayas to 17°N. The depth of the westerlies which is about 7 km at the equator, shows a slight decrease northward upto about 17°N but increases rapidly thereafter reaching 10 km at 35°N. The overlying easterlies extend upto the maximum level considered (35 km).

Fig. 6 shows the vertical cross-section of the observed mean zonal wind during July from equator to 40°N, which is prepared from an analysis

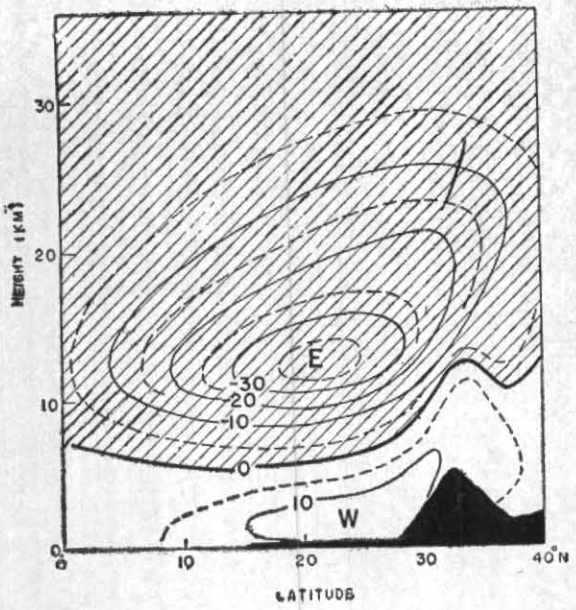

Fig. 5

Vertical cross-section of simulated zonal wind u (m sec^{-1}) along 80°E for wet model with the Himalayas

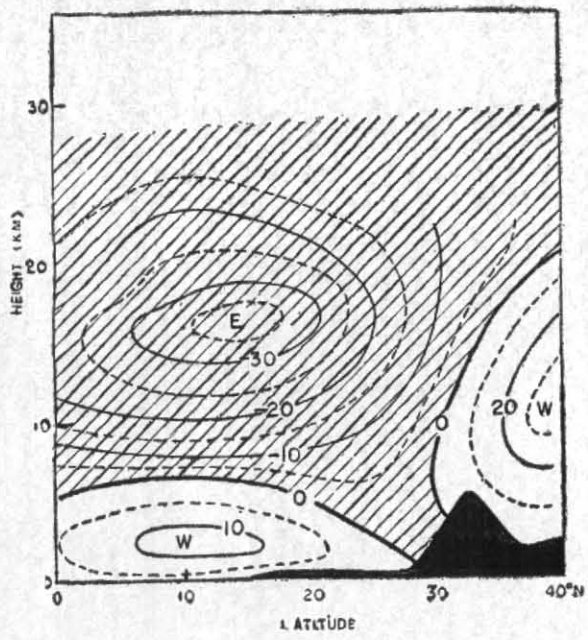

Fig. 6

Vertical cross-section of observed zonal wind u (m sec^{-1}) along 80°E

Easterly regime (E) is hatched

by Godbole (1971). The analysis above 100 mb is based on the available data for 40 and 30 mb, being supplemented by the results of Flohn (1964) and Koteswaram (1969). Comparison of Figs. 5 and 6 points out an agreement between the simulated and the observed wind pattern in so far as the main features are concerned, *i.e.*, the upper level easterlies with TEJ and the low-level westerly flow to the south of the Himalayas. However, the increasing tendency in the depth of the westerly with latitude northward from 17°N indicated by the simulated pattern is absent in the observed wind pattern. Instead, its depth in the observed pattern, decreases progressively with latitude from equator to 30°N.

The vertical cross-section of the simulated meridional wind is shown in Fig. 7. In the lower troposphere, the wind is southerly with a maximum speed of 4·3 m sec^{-1} near the surface. In the upper troposphere and lower stratosphere (upto 20 km) northerly wind with a maximum speed of 2 m sec^{-1} prevails. The northerly extends even into the middle stratosphere (upto 30 km). Thus, the simulated pattern south of the Himalayas exhibits the features of direct circulation cell as characterised by southerlies below and northerlies aloft. This circulation has been identified as the monsoon cell.

The vertical cross-section of the observed meridional component of wind is shown in Fig. 8 which was prepared from the analysis by Godbole (1971). A southerly wind was observed near the surface and in the middle troposphere, and a northerly wind in the lower and in the upper troposphere. Comparison with Fig. 7 shows that the simulated northerly wind is weaker than the observed. Also, the northerly which is observed in the middle troposphere is absent in the simulated wind field.

In Fig. 9 is shown the distribution of the simulated temperature with respect to height and latitude. The air in the region above the Himalayas is warmer than that over the equatorial regions considered at the same level. This is due to reabsorption of reflected solar radiation which itself is large due to higher albedo for the Himalayas as compared to the surrounding. The higher temperatures indicated northward are consistent with the strong and upward increasing tropospheric easterlies noticed over India (Koteswaram 1960).

The other conspicuous features brought out by the simulated temperature field are: (*i*) the temperature at the tropopause level is minimum over the Himalayas, and (*ii*) the height of the tropopause increases with latitude. For comparison a vertical cross-section of mean July temperature field has been presented from the temperature analysis by Godbole (1971). The results which are shown in Fig. 10 and also the findings of Sastry *et al.* (1966) and Sivaramkrishnan *et al.* (1972) are in agreement with those obtained by simulation. The difference between the maximum and

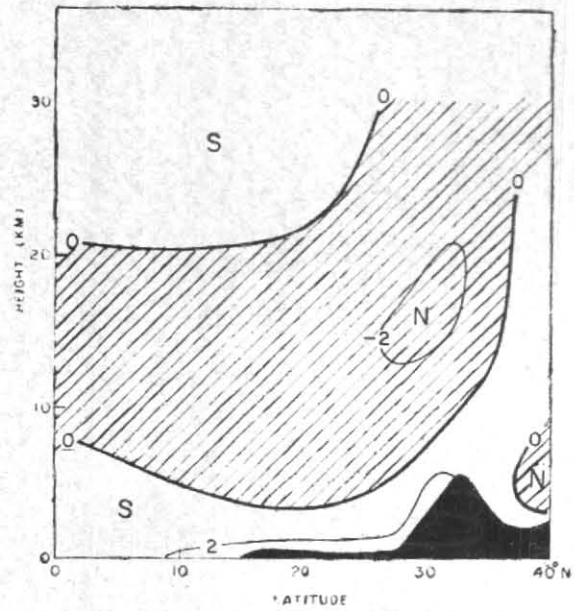

Fig. 7. Simulated meridional wind v (m sec^{-1})

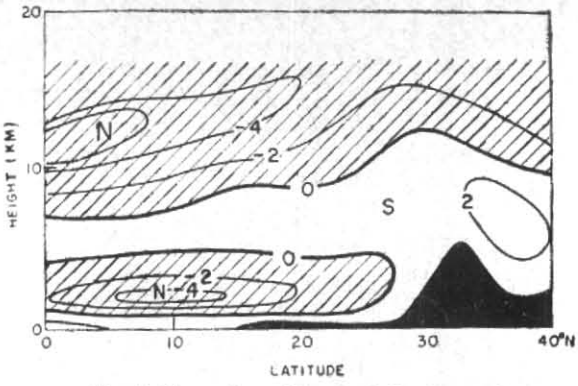

Fig. 8. Observed meridional wind v (m sec^{-1})

Northerly regime (N) is hatched

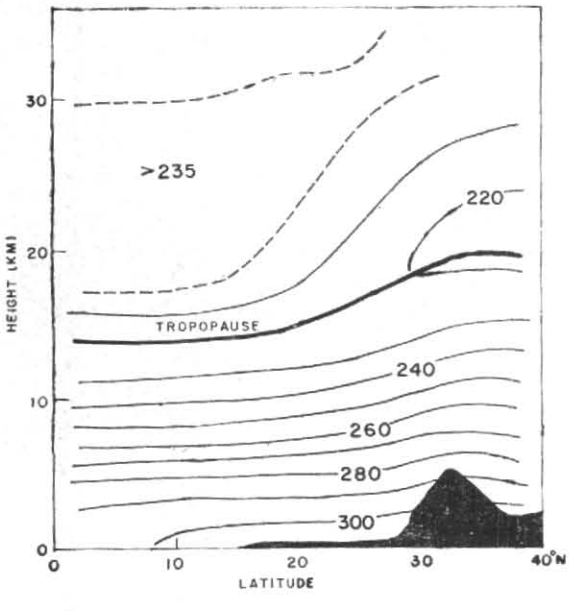

Fig. 9. Simulated temperature (°K)

Figs. 7 & 9. Vertical cross-section along 80°E for wet model with the Himalayas

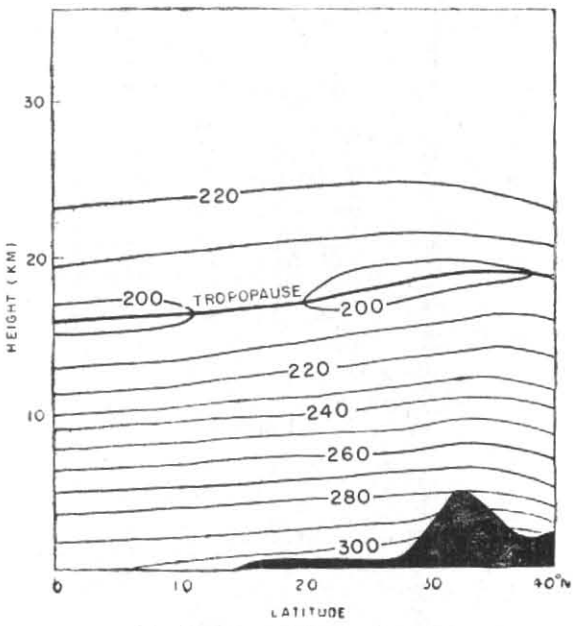

Fig. 10. Observed temperature (°K)

Figs. 8 & 10. Vertical cross-section along 80°E

minimum tropopause height in the computed pattern (Fig. 9) is, however, very large when compared with the observed pattern (Fig. 10). In any case, these features are at variance with global mean temperature cross-section given by London *et al.* (1957) for July. The findings, therefore, point out that the conventional global features available in the literature are not applicable for the Indian longitudes where the presence of the Himalayas exercise considerable influence on the monsoon circulation.

The variation of tropopause height with latitude is mainly due to radiative processes. The vertical profiles (not shown) of water vapour mixing ratio, on the basis of which Fig. 3 was prepared, show that, in the region south of the

TABLE 1

Ocean-continent temperature contrast ($\triangle T$°C) between 2·5°N and 27·5°N

Level (K)	Pressure (mb)	With the Himalayas with sea surface temperature at 300°K		Without the Himalayas with sea surface temperature at	
		Wet model	Dry model	300°K	290°K
9	Surface	13·2	33·2	21·9	29·4
8	955	8·1	22·1	9·9	13·8
7	855	5·1	11·2	4·7	6·4
6	710	4·1	3·7	0·7	1·0
5	540	4·0	3·1	0·4	0·5
4	367	11·2	1·4	0·3	0·9
3	208	13·2	11·0	0·3	0·4
2	82	—13·0	—11·6	0·3	0·4
1	10	—1·4	2·3	0·6	0·9

Himalayas, high latitudes have more amount of water vapour penetrating to greater heights than low latitudes. The result is that cooling due to water vapour penetrates correspondingly to greater heights pushing the tropopause upward over high latitudes when compared with low latitudes (Godbole *et al.* 1971).

10.2. *Dry model with the Himalayas*—As the atmosphere is assumed to be dry, there is no evaporation at the earth's surface and no condensation in the atmosphere. The results are shown in Fig. 11 in which the zonal wind is plotted with respect to height and latitude. Comparison with Fig. 5 (wet model with the Himalayas) shows that there is no pronounced difference between the configurations of the two wind fields. The winds obtained by the dry model are slightly weaker than those obtained by the wet model. The core speed of the easterly jet decreases from 30 m sec^{-1} in the wet model (Fig. 5) to 25 m sec^{-1} in the dry model (Fig. 11). The low level westerly also decreases from 14 m sec^{-1} to 12 m sec^{-1}.

10.3. *Dry model without the Himalayas* — The atmosphere was assumed to be dry, as in the earlier experiment. In addition, the presence of the Himalayas was not taken into account. The experiment has been performed, as already stated, for two sea surface temperatures, namely, 300°K and 290°K.

(a) *Sea surface temperature at 300°K* — The vertical cross-section of the zonal wind component

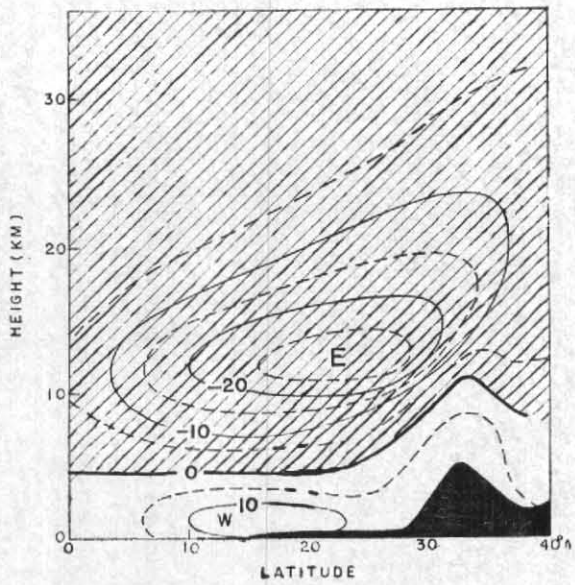

Fig. 11

Vertical cross-section of simulated zonal wind u (m sec^{-1}) along 80° E for dry model with the Himalayas. Easterly regime (E) is hatched

simulated is shown in Fig. 12 . In the region to the south of 25° N, the westerly current prevails in the lower levels while an easterly flow exists aloft, and the height of the boundary between the westerly and the easterly decreases northward in the manner as observed. It may be emphasised, therefore, that one of the important characteristic features of the monsoon circulation, *i.e.*, the westerlies in the lower troposphere capped by the easterlies aloft, has been qualitatively simulated even by using a simplified model. But the circulation indicated is weak, especially, in the upper troposphere. Comparing Fig. 12 (simulated) with Fig. 6 (observed) it is seen that in place of the tropical easterly jet (TEJ) with core speed of 35 m sec^{-1}, there has been a very weak easterly simulated with core speed of only 8 m sec^{-1}. Similarly, the intensity of the westerly simulated is less than the observed strength by a factor of three. The depth of the westerly generated is also 2 to 3 times smaller than the observed.

(b) *Sea surface temperature at 290° K* — The vertical cross-section of zonal wind obtained is illustrated in Fig. 13. Comparison of features as seen in Figs. 12 (for sea surface temperature at 300°K) and 13, points out that there is practically no difference in the pattern obtained either with respect to the depth and the extent of the westerlies or the strength and the location of the easterlies. The circulation with sea surface temperature at 290° K is slightly stronger (easterly core speed of 9 m sec^{-1}) than that with sea surface temperature at 300°K (easterly core speed of 8 m sec^{-1}).

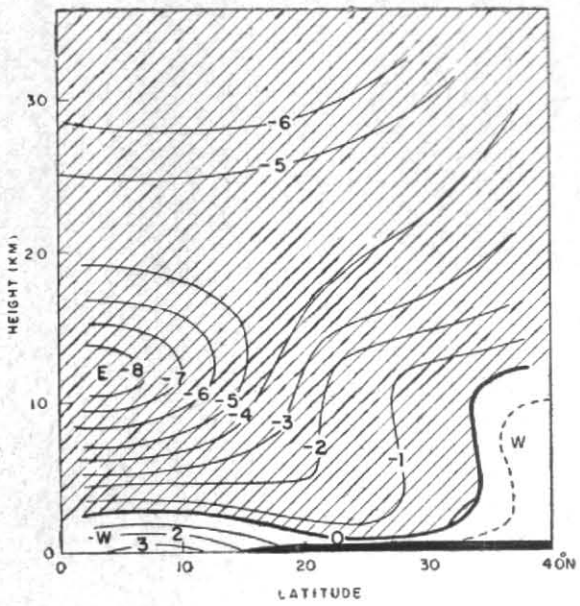

Fig. 12

Vertical cross-section of simulated zonal wind u (m sec^{-1}) along 80°E for dry model without the Himalayas with sea surface temperature fixed at 300°K. Easterly regime(E) is hatched.

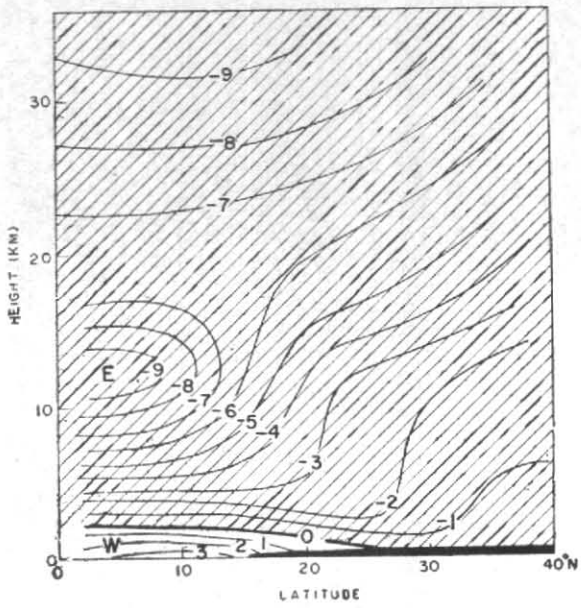

Fig. 13

Vertical cross-secton of simulated zonal wind u (m sec^{-1}) along 80° E for dry model without the Himalayas with sea surface temperature fixed at 290°K. Easterly regime (E) is hatched

The ocean-contenent temperature contrast obtained in the foregoing wet and dry model experiments is shown in Table 1. The values of the temperature contrast obtained in the dry model experiments without the Himalayas are considerably smaller than those in the wet and dry model experiments with the Himalayas as far as the upper tropospheric levels (above 700 mb) are concerned. The absence of the easterly jet in the experiments without the Himalayas is due to the absence of strong thermal winds in the upper troposphere, *i.e.*, between 300 and 100 mb. For example, at 208 mb the temperature contrast is only 0·3 and 0·4° C in the experiments without the Himalayas as against 13·2 and 11·0°C in the experiments with the Himalayas. The models considered without the Himalayas, therefore, lead us to infer that the monsoon circulation as observed cannot be simulated until the north-south temperature contrast on the mean attains a value of not less than 0·5°C per degree latitude in the upper troposphere.

It is also seen from Table 1 that the ocean-continent temperature contrast in the dry model experiments is large (more than twice, in some cases) when compared with values in the wet model experiment. The main reason for this is that in the dry model experiment the process of evaporation, which acts as a heat sink, is missing; consequently, the entire available heat is used up in warming the atmosphere. The presence of moisture would, on one hand, tend to decrease the temperature of the lower layers through evaporation and, on the other hand, increase the temperature of the middle troposphere through condensation. In the following experiments, the role of moisture in the monsoon circulation has been examined.

10·4. *Wet model without the Himalayas* — The presence of moisture in the air is taken into account but not the presence of the Himalayas. Three cases have been considered as already stated : (a) water vapour mixing ratio at the surface is 80 per cent ($\beta = 0{\cdot}8$ in equation 9·1) of the saturation mixing ratio at the surface, (b) water vapour mixing ratio is 40 per cent ($\beta = 0{\cdot}4$ in equation 9·1) of the saturation mixing ratio at the surface, and (c) condensation occurs at 80 per cent relative humidity instead of at 100 per cent with the evaporation rate remaining as in (b). In experiments (a) and (b), condensation is assumed to take place only at 100 per cent relative humidity.

(a) *Surface mixing ratio at 80 per cent* — In Fig. 14 is shown the vertical cross-section of the simulated zonal wind. The monsoon circulation generated is weak as compared to that generated in the case of dry model without the Himalayas (Fig. 12). The upper level easterly decreases from 8 m sec^{-1} in the dry model to 3 m sec^{-1} in the present wet model, while the low-level westerly decreases from 3 m sec^{-1} to 2 m sec^{-1}.

(b) *Surface mixing ratio at 40 per cent* — The results obtained are presented in Fig. 15. The circulation becomes strong as compared to what it is for $\beta = 0{\cdot}8$ (Fig. 14). The upper level easterly

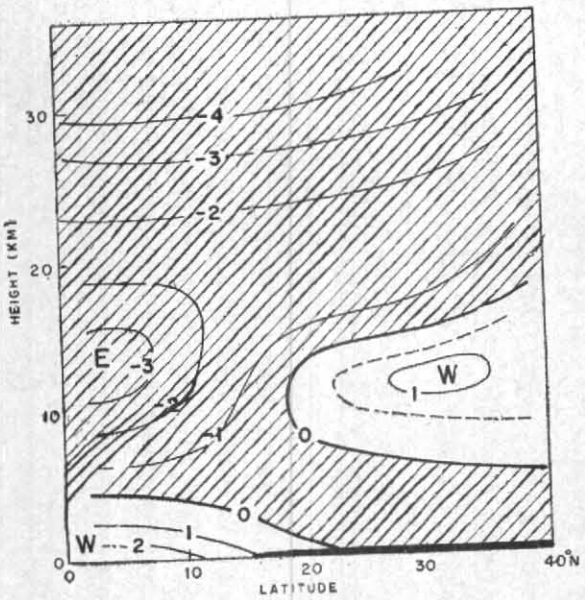

Fig. 14

Vertical cross-section of simulated zonal wind u (m sec^{-1}) along 80°E for wet model without the Himalayas with $\beta=0{\cdot}8$. Easterly regime (E) is hatched.

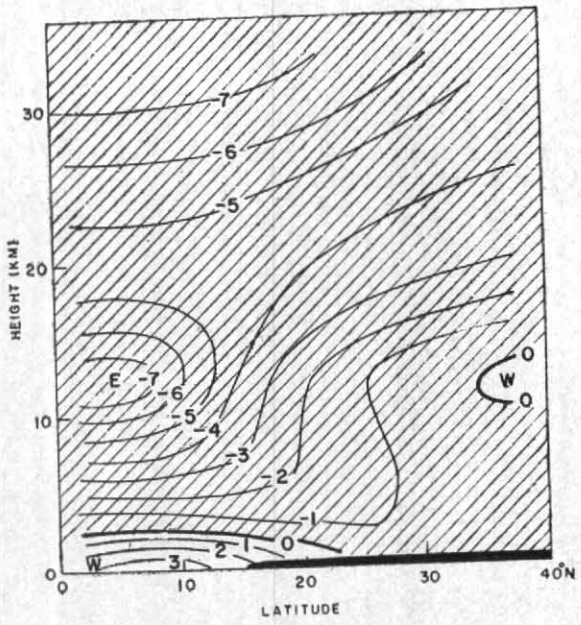

Fig. 15

Vertical cross-section of simulated zonal wind u (m sec^{-1}) along 80°E for wet model without the Himalayas with $\beta=0{\cdot}4$. Easterly regime (E) is hatched.

increases to 8 m sec^{-1} and the low level westerly to 3 m sec^{-1} as in the dry model without the Himalayas (Fig. 12).

The features noticed as in (a) and (b) may be accounted for as follows. More injection of moisture from the ground ($\beta=0{\cdot}8$) as in (a) demands more absorption of latent heat of vaporization which, in effect inhibits building up of ocean-continent temperature contrast (*vide* Table 2). Such a build-up is one of the factors responsible for the development of strong circulation. In addition, more moisture content injected into the air from the ground (when $\beta=0{\cdot}8$) does not guarantee correspondingly more release of latent heat of condensation in the middle troposphere (*vide* Table 3). But when $\beta=0{\cdot}4$ as in (b), the less evaporation rate consequent at the ground favours building up of strong ocean-continent temperature contrast (Table 2). The circulation in (b), therefore, become stronger.

The results of the experiments (a) and (b) above are of importance, because they suggest an explanation of the well-known observational fact, namely, why there is no monsoon type circulation over the Pacific and the Atlantic. The differential distribution of land and sea in the north-south as over the Indian Ocean longitudes is not present over the longitudes of the Pacific and the Atlantic. Since the evaporation rate which is maximum over the oceans, does not differ appreciably from north to south, the necessary north-south temperature contrast for the monsoon-type circulation never builds up over these regions.

(c) *Condensation at 80 per cent relative humidity* — It is known that condensation in the atmosphere takes place well before 100 per cent relative humidity is actually reached. Following Smagorinsky *et al.* (1965), the condensation criterion was set to 80 per cent instead of 100 per cent relative humidity. This would help reduce the allowed storage of water vapour in the free atmosphere and consequently release additional amount of condensation heat.

Fig. 16 shows the simulated zonal wind pattern. The results point out that the monsoon circulation with condensation criterion of 80 per cent relative humidity (Fig. 16) remains practically unchanged from that with condensation criterion of 100 per cent relative humidity (Fig. 15). On the contrary, the circulation in Fig. 16 shows an indication of slight weakening when compared to that in Fig. 15. It may be noted that Miyakoda *et al.* (1969) in their two-week prediction experiment also arrive at a similar results, namely , that the tropical Hadley cell is weaker with a condensation criterion of 80 per cent relative humidity.

10.5. *Role of evaporation and condensation* — Quantitative information about precipitable water from equator to north pole and precipitable water from equator to 42·5°N as obtained in the foregoing wet model experiments is presented in Table 3. The values in the table are comparable

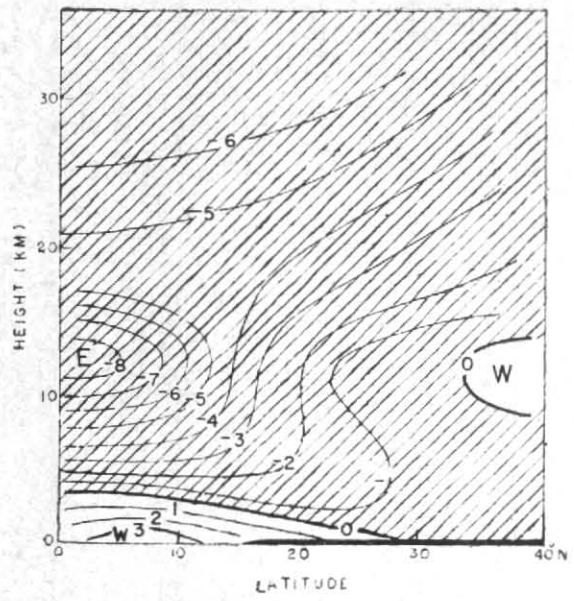

Fig. 1c

Vertical cross-section of simulated zonal wind u (m sec^{-1}) along 80°E for wet model without the Himalayas with condensation at 80% relative humidity and with $\beta=0\cdot4$. Easterly regime (E) is hatched.

TABLE 2

Ocean-continent temperature contrast ($\triangle T$°C) between 2·5°N and 27·5N

Level (K)	Pressure (mb)	Wet model: With the Himalayas R.H. 100% $\beta=0\cdot8$	Wet model: Without the Himalayas R.H. 100% $\beta=0\cdot8$	Wet model: Without the Himalayas R.H. 100% $\beta=0\cdot4$	Wet model: Without the Himalayas R.H. 80% $\beta=0\cdot4$
9	Surface	13·2	5·6	15·1	14·8
8	955	8·1	1·8	7·8	5·7
7	855	5·1	1·8	3·8	3·4
6	710	4·1	0·1	0·8	0·9
5	540	4·0	—0·2	0·6	0·6
4	367	11·2	—0·7	0·5	0·5
3	208	13·2	—0·2	—0·2	—0·4
2	82	—13·0	0·9	0·7	0·7
1	10	—1·4	0·7	0·6	0·7

TABLE 3

Precipitable water and precipitated water for wet model experiments. The values represent integrated amount from the surface to the top of the atmosphere

	With the Himalayas R.H. 100% $\beta=0\cdot8$	Without the Himalayas R.H. 100% $\beta=0\cdot8$	Without the Himalayas R.H. 100% $\beta=0\cdot4$	Without the Himalayas R.H. 80% $\beta=0\cdot4$
Precipitable water Equator to north pole 10^{16} gm/longitude	268	263	231	248
Precipitated water Equator to 42·5°N 10^{16} gm/day	0·11958	0·00709	0·02192	0·01832

with those obtained by Subbaramayya *et al.* (1966) for precipitated water, and by Godbole *et al.* (1969) for precipitable water. It is seen that the precipitable water in the models with $\beta=0\cdot8$ is more than that with $\beta=0\cdot4$ which is consistent. What is more interesting is the fact that the total amount of condensate (precipitated water) becomes less for condensation criterion at 80 per cent relative humidity ($0\cdot01832\times10^{16}$ gm) than at 100 per cent ($0\cdot02192\times10^{16}$ gm). It is this feature which is responsible for the lower values obtained of the ocean-continent temperature contrast at 80 per cent relative humidity than at 100 per cent (Table 2), and consequently weakening the circulation (Fig. 16). Table 3 also reveals that the total amount of condensate is less for higher evaporation rate (*vide* figures in columns 3 and 4 against precipitated water). The lower values of the ocean-continent temperature contrast obtained with $\beta=0\cdot8$ than with $\beta=0\cdot4$ (Table 2) and the resulting weakening of the circulation (Fig. 14) are due to this feature.

The values obtained for the total amount of condensate in the model with the Himalayas ($0\cdot11958\times10^{16}$gm) which is about five times more than those in the other models without the Himalayas speaks about the dominent role of the Himalayas in the shaping of rainfall and circulation patterns of the Indian summer monsoon.

11. Conclusions

(1) In the wet model with the Himalayas, the simulated TEJ has a core speed of 36 m sec^{-1} at a height of 12 km at 20°N as against the observed TEJ with a core speed of 35 m sec^{-1} at 14 km at 15°N.

(2) In the dry model with the Himalayas, the simulated circulation pattern remains unchanged as in (1). The TEJ has a core speed of 25 m sec^{-1}.

(3) The presence of high amounts of moisture at the surface tend to decrease the intensity of the monsoon circulation. Higher amounts of moisture at the surface contribute only to higher amounts of precipitable water but not to preciptiated water.

(4) Results with wet and dry model experiments lead to the inference that moisture is not the important factor in controlling the monsoon circulation, although it is essential for the occurrence of rainfall.

(5) Experiments with and, without the Himalayas lead to the conclusion that *it is the presence of the Himalayas which has the dominent effect upon the development of the monsoon circulation.*

(6) The pattern of the simulated temperature field is similar to that of the observed temperature field. Also, the height, of the tropopause, south of the Himalayas increases with latitude in accordance with what is observed.

(7) The monsoon circulation would develop in the manner it is observed only if the horizontal thermal gradient is more than 0·5°C per degree latitude *in the upper troposphere.*

(8) A marked decrease in the Indian Ocean surface temperature by as much as 10°C does not significantly change the monsoon circulation both in its pattern and intensity.

(9) The distribution of land and sea in the north-south as exists over the Indian Ocean longitude is one of the essential factors for the development of this monsoon.

The model used in the present investigation is zonally symmetric and hence it operates only in the two-dimensional vertical plane along any longitude which is 80° E in the present model. The present investigation, therefore, cannot answer some of the important questions, such as, the interaction between the northern and southern hemispheres, the role of westward or eastward moving depressions, and the importance of the Western Ghats. A complete ocean-atmosphere model taking into account the advection of heat by ocean currents and sea-upwelling and with topographic features including the Western Ghats, will certainly help understand the basic processes of diabatic heating and cooling and their importance in the genesis and development of the monsoon.

Acknowledgements

The author wishes to express his sincere thanks to Dr. Bh. V. Ramana Murty for his interest in the study and for making many useful suggestions. Thanks are due to Dr. T. Murakami, who during his tenure as WMO Expert in the Institute initiated the author to the present study, to Shri K. Krishna for having useful discussions, and to Dr. R.R. Kelkar for his valuable assistance in computer programming and its execution. Thanks are also due to Shri Girijavallabhan for typing the manuscript and to our colleagues in the Drawing Section for their help in preparing the diagrams.

REFERENCES

Flohn, H. 1964 Investigation on the Tropical Easterly Jet. *Meteor. Inst. der Univ. Bonn*. Heft **4**, 83 pp.

Godbole, R. V. 1971 Climatology and Simulation of Indian Summer Monsoon, *Ph.D. Thesis*, pp. 26-54.

Godbole, R. V. and Kelkar, R. R. 1969 *Indian J. met. Geophys.*, **20**, pp. 1-10.

1971 *Ibid.*, **22**, pp. 161-168.

Godbole, R. V., Kelkar, R. R. and Murakami, T. 1970 *Ibid.*, **21**, pp. 43-52.

Holloway, J. L. Jr., and Manabe, S. 1971 *Mon. Weath. Rev.*, **99**, pp. 335-370.

Koteswaram, P. 1960 *Monsoons of the World*, India met. Dep., New Delhi pp. 105-110.

REFERENCES (contd)

Koteswaram, P.	1969	Forecasting of Upper Winds and Temperature in Tropical Latitudes with special reference to Jet Streams. *Aeronautical Met. Tech. Note.*, 95, WMO-No 227-TP 121, pp. 218-228.
Kurihara, Y. and Holloway, J. L.	1967	*Mon. Weath. Rev.*, **95**, pp. 509-530.
Leith, C.	1965	Numerical Simulation of the Earth's Atmosphere. *Methods in Computational Physics*, **4**. Academy Press, New York.
London, J., Ohring, G. and Ruff, I.	1956	Radiative Properties of the Stratosphere. *Final Rep. Res. Div. College of Engg.*, N.Y. Univ., 48 pp.
Manabe, S. and Moller, F.	1961	*Mon. Weath. Rev.*, **89**, pp. 503-532.
Manabe, S., Smagorinsky, J. and Strickler, R. F.	1965	*Ibid.*, **93**, pp. 769-798.
Manabe, S., Holloway, J. L. Jr. and Stone, H. M.	1970	*J. atmos. Sci.*, **27**, pp. 580-613.
Mintz, Y.	1965	The Seasonal Variations in a Numerical General Circulation Experiment, *Proc. Int. Symp. Large-Scale Processes*, Moscow.
Mintz, Y. and Arakawa, A.	1963	Long Term Numercial Investigation of the Equations of Atmospheric Motions over the entire Globe. *Proc. Int. Symp. Large-Scale Processes*, Boulder.
Miyakoda, K., Smagorinsky, J. Strickler, R. F. and Hembree, G. D.	1969	*Mon. Weath. Rev.*, **97**, pp. 1-76.
Murakami, T., Godbole, R. V. and Kelkar, R. R.	1968	Numerical Experiment of the Monsoon along 80°E Longitude. *Sci. Rep.*, 62, India met. Dep., I.T.M. Poona, 51 pp.
Murgatroyd, R. J.	1964	Ozone and Water Vapour in the Upper Troposphere and Lower Stratosphere. *WMO Tech. Note*, 169 TP-83. pp. 68-69.
Phillips, N.	1956	*Quart. J.R. met. Soc.*, **82**, pp. 123-164.
Ramanathan, K. R. and Kulkarni, R. N.	1960	*Ibid.*, **86**, pp. 151-155.
Sastry, P. S. N. and Narasimham, A. L.	1966	*Indian J. Met. Geophys.*, **17**, pp. 567-572.
Sivaramakrishnan, M. V., Mokashi, R. Y. and Parameswaran, N. V.	1972	A Study of Tropopause over India *Sci. Rep.*, 171. India met. Dep., Poona. 7 pp.
Smagorinsky, J., Manabe, S. and Holloway Jr. J. L.	1965	*Mon. Weath. Rev.*, **93**, pp. 727-768.
Subbaramayya, I. and Ramanadham, R.	1966	*J. met. Soc. Japan*, **44**, pp. 167-172.
U.S. Air Force	1962	*U.S. Standard Atmosphere*, Govt. Printing Office, Washington.